2D Image Construction from Low Resolution Response of a New Non-invasive Measurement for Medical Application

Ichiro Hieda and Ki-Chang Nam

This paper presents an application of digital signal processing to data acquired by the radio imaging method (RIM) that was adopted to measure moisture distribution inside the human body. RIM was originally developed for the mining industry; we are applying the method to a biomedical measurement because of its simplicity, economy, and safety. When a two-dimensional image was constructed from the measured data, the method provided insufficient resolution because the wavelength of the measurement medium, a weak electromagnetic wave in a VHF band, was longer than human tissues. We built and measured a phantom, a model simulating the human body, consisting of two water tanks representing large internal organs. A digital equalizer was applied to the measured values as a weight function, and images were reconstructed that corresponded to the original shape of the two water tanks. As a result, a two-dimensional image containing two individual peaks corresponding to the original two small water tanks was constructed. The result suggests the method was applicable to biomedical measurement by the assistance of digital signal processing. This technique may be applicable to home-based medical care and other situations in which safety, simplicity, and economy are important.

Keywords: Radio imaging method, RIM, medical imaging, tomography, weight function, digital equalizer.

Manuscript received Feb. 3, 2004; revised Mar. 24, 2005.

Ichiro Hieda (phone: +81 29 861 9430, email: i-hieda@aist.go.jp) is with AIST, Japan.

Ki-Chang Nam (email: chadol@yumc.yonsei.ac.kr) is with the Department of Medical Engineering, Yonsei University, Korea.

I. Introduction

We have developed a new biomedical measurement method that creates an image of the inside of a patient's body by active application of weak electromagnetic waves. For decades, nondestructive measurement techniques employing electromagnetic waves have been developed. Application of these measurement techniques is not limited to medicine, and many are in practical use today. Generally, the shorter the wavelength, the finer the resolution becomes. Therefore, for medical devices, microwaves are usually used [1], [2]. However, the shorter the wavelength, the less penetration of the body occurs [3], [4]. An antenna having high gain and a sharp beam pattern is necessary for transmitting or receiving, or under some circumstances, for both transmission and reception. At the same time, electromagnetic waves are reflected by the surface of a body. Shielding, or an electromagnetic darkroom with walls that absorb electromagnetic waves of the measurement frequency, is necessary to compensate for these weaknesses. Thus, the simplicity and economy offered by methods using electromagnetic waves is lost.

Among nondestructive inspection methods that use electromagnetic waves, a radio imaging method (RIM) has been developed for geological surveying, and is still used today [5]-[9]. It uses very low frequency electromagnetic waves from tens of kilohertz to several hundred kilohertz (LF band) and possesses the following characteristics: a) the electromagnetic waves are capable of penetrating the measurement medium, and b) reflection of the electromagnetic waves is not a significant problem.

Small omnidirectional loop antennas are used so that the antennas are small enough to move through boreholes. Initially, because the velocity of electromagnetic waves through the measurement medium is slower than in free space, the wavelengths become shorter but are still not small enough to achieve the needed resolution. To eliminate this drawback, a system used to process tomography was linked to a database of geological features.

We have applied a basic principle of RIM to biomedical engineering [10]-[12]. Figure 1 is a conceptual diagram of the measurement method. The subject or the antenna is moved and rotated to allow scanning of the subject by weak electromagnetic waves. This method offers the advantages of simplicity and economy. No high-tech element is involved, except in the image reconstruction. Radiation power of the experimental system is estimated around tens of mW, smaller than that of mobile phones. By improving the total performance of the system, the radiation power can be reduced, contributing to an increase in safety.

Another advantage of the proposed method is elimination of the need to attach electrodes to the skin, unlike in ECG, EMG, or bio-impedance methods. Thus, no stimulus, inflammation, or other discomfort to the skin is created, which is an advantage for use at home.

The basic measurement method is based on the RIM of geological surveys. However, the dimensions of the subjects differ by several hundred to several thousand times, and the physical properties of the subjects also differ. These differences required addressing when to apply the method to the measurement of a living human body.

The project had two goals. One was the development of computerized tomography that had as fine a resolution as possible. From the measured signal strength, the system creates images of internal structures in sub-real time. The second goal was the development of real-time biomedical devices that could monitor functions necessary for effective home medical care, such as blood flow, lung function, hydration status, and bladder urinary volume. However, improvement of the resolution of the basic method was a primary purpose.

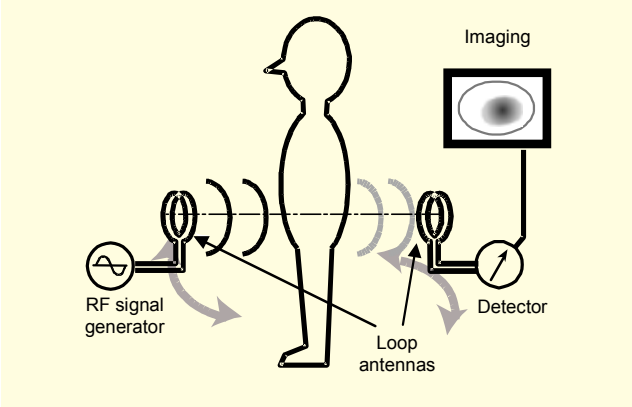

Fig. 1. Overview of biomedical imaging by RIM.

One of the essential elements of this study was to discover the optimal frequency. The higher the frequency, the finer is the expected resolution. However, electromagnetic waves of high frequency also reflect off of the surface of the body, causing considerable disturbance. In consideration of the dimensions of a living body, preliminary experiments began at 1.2 GHz, resulting in a wavelength of 25 cm in free space and a wavelength of approximately 3 cm in the human body. These conditions were expected to provide resolution equivalent to that obtained by bio-impedance tomography [13]-[15]. However, results of pilot experiments revealed that electromagnetic waves at the frequency obtained did not penetrate deeply enough into the body for effective measurement, and that reflections were a significant problem.

Therefore, the experiments were repeated while reducing frequency in a step-wise manner. When a small loop antenna w as operated at 54 MHz in the VHF band, measurements were obtained successfully for both a living human body and a water tank that simulated the moisture distribution within the human body. At this frequency, losses caused by eddy current and other factors were not dominant. Instead of the losses, improvement of electric field intensity was measured, which was caused by large permittivity of water. Special shielding was not necessary in the measurement environment. Experiments continued using the specially designed water tank that simulated the human body.

A previous paper [12] introduced basic experiments where signal strength was measured under three conditions: when the inner tank only was filled with water, the outer tank only was filled with water, and both inner and outer tanks were filled with water. The initial back projections were blurred images in the shape of the water tank. However, results indicated a significant difference could be detected between when the inner tank was filled with water and when it was empty. Results also showed that the signal strengths could be added and subtracted to yield linear results. The resolution of the measurement system was discussed in terms of spatial frequency.

In this study, original shapes were estimated from the blurred signals by applying a digital equalizer used in communication engineering. A small water tank of simple structure was used as a known reference. Results from the digital equalizer were calculated from responses measured off of the reference water tank. The equalizer was applied to a phantom consisting of two side-by-side water tanks as an unknown subject to test the ability of the method to accurately reconstruct the two-dimensional image from the measured values.

II. Methods

1. Antennas and RF Generator

In all experiments, antennas fixed on thin wooden stands were kept 30 cm apart and the center of each antenna was set 900 mm off the floor. Water tanks were constructed using a 5 mm acrylic board and placed on an acrylic stand. The water tanks were conducted between the two antennas by a stepper motor located on the floor to minimize any disturbance of the mechanism to the measurement field.

The transmitting and receiving antennas had similar structures, as shown in Fig. 2. The antennas were constructed of coated copper wire with a diameter of 1 mm. Each antenna consisted of 10 turns of the wire and a loop with a diameter of 40 mm. A balance-unbalance transformer or "balun" with a permeable toroidal core was inserted at each feeding point to suppress unnecessary emission to or receipt by the coaxial cables [16]. The output power of the RF generator was 200 mW (23 dBm) and the frequency was 54 MHz. The antenna did not have regular impedance, and the voltage standing wave ratio measured approximately 14 at this frequency. The transmitted electric power was estimated at 10 mW.

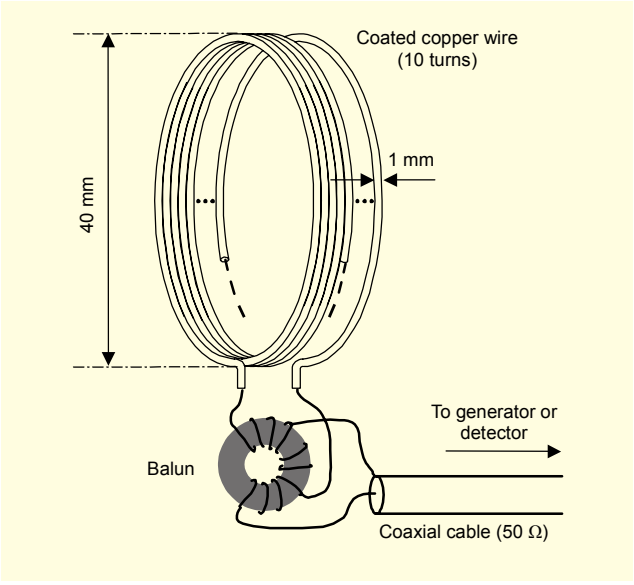

Fig. 2. Schematic diagram of loop antenna and feeding system.

2. RF Measurement

Signal strength of the fundamental frequency, 54 MHz, was measured by an Anritsu MS2621B spectrum analyzer. The relation between the measured value and absolute electric field intensity was not calibrated. The stability of the transmission and measurement system were tested by continuous measurement at 5 minute intervals for ten hours without a subject, which confirmed system stability.

3. Measurement of Reference Water Tank

Water tanks were used as models that simulate the distribution of moisture inside of a living human body. Previous studies revealed that losses caused by eddy currents in water were too small to be measured. However, the dominant effect caused the water to develop an electric field intensity. In the study we also examined pure water, a saline solution of various densities including physiological saline, and tap water. However, no clear differences among the types of water existed. Therefore, tap water was used for convenience [12]. The effect of the tank material was insignificant because the volume and permittivity of the tank material were small in comparison to that of water. The relative permittivity of the tank material was approximately 3.0, and that of water was approximately 70, each at 54 MHz [15].

The inside dimensions of the reference tank were 80 mm × 60 mm × 280 mm, and it was filled to a height of 250 mm with water, as shown in Fig. 3. The tank was mounted on the measurement platform. The center of the water height was 900 mm from the floor, which corresponded to the central height between the pair of antennas.

Figure 4 shows a top view of the measurement plane. The water tank moved along Paths 1 to 9, and each distance between neighbor paths was 20 mm except the distance to Path 5. The distances between Paths 4, 5 and 6 were 10 mm. Signal strength was measured at every 20 mm step on each path. The water tank was measured at 33 points within a 640 mm span on each path, giving a total number of measurement points of 297. The water tank moved forty times along each path, resulting in forty measurements at each point.

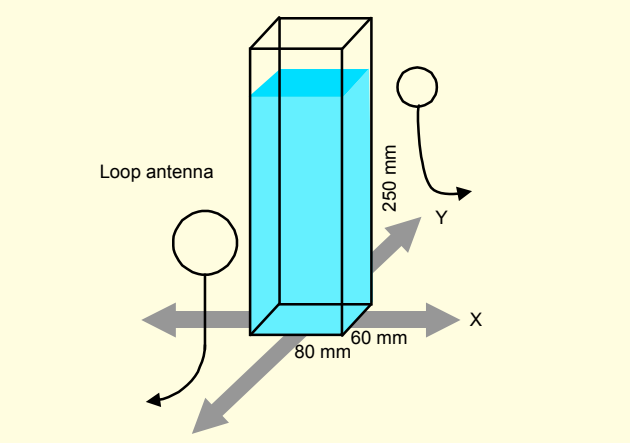

Fig. 3. Schematic diagram of water tank used for the reference measurement.

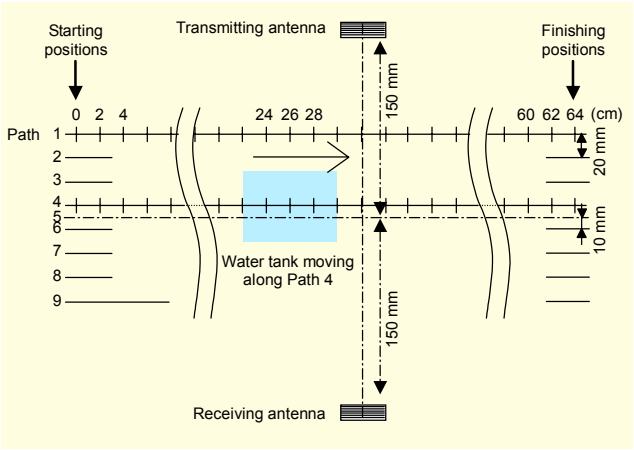

Fig. 4. Top view of measurement paths and positions for the reference measurement.

4. Major Experiment

For the main measurement, two water tanks with horizontal sections of 80 mm × 60 mm were used. One was filled to a height of 250 mm, the other to a height of 125 mm, as shown in Fig. 5(a). The two tanks remained fixed as shown in Fig. 5(b). The upper and lower figures represent top and front views, respectively. The water tanks were placed on a stand to align the center heights of the tanks and the antennas, which were 900 mm from the floor.

The water tank used in these experiments had a smaller cross section than did the water tank used previously. Because initial studies demonstrated that addition and subtraction of measurement results with and without water was possible [12], measurement of a small water tank was complement to that of the larger water tank with inner cavities that simulated a human body.

In this report, preliminary studies were designed to recreate two-dimensional images of tanks representing large internal organs such as the urinary bladder. These studies yielded electric field intensity curves that corresponded to a back projection of a square water tank. However, fine resolution was not expected from these studies. The goal of the study conducted here was successful discrimination of the two water tanks in the two-dimensional image. The tanks were not scanned in the vertical direction, although this might result in height discrimination if their heights are different.

Figure 6 shows a top view of the measurement plane. The pair of tanks moved on the center line between the two antennas. The tanks were turned by π 8th radian (or 22.5°) after a set of measurements, resulting in 16 measurement directions. The center point of the tank rotation always moved along the measurement path. Signal strength was measured at every 20 mm step on a 640 mm long measurement path, yielding 33 points. Twenty measurements were taken for every condition.

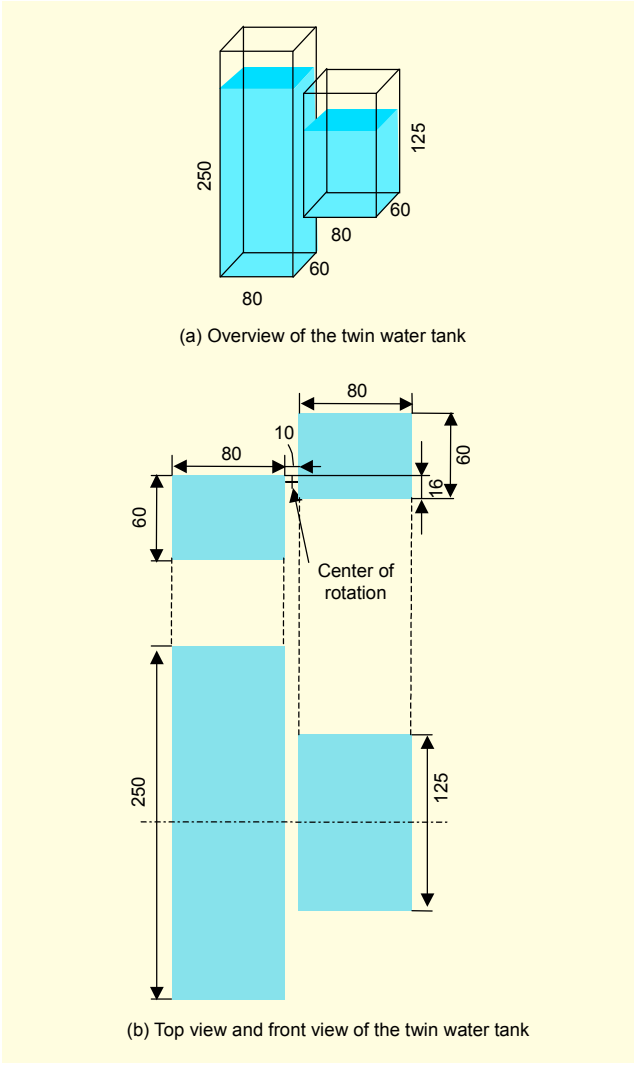

Fig. 5. Schematic diagram of the twin water tank.

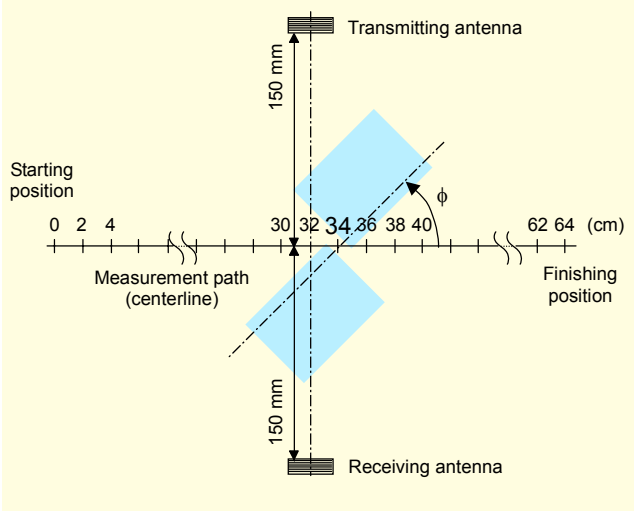

Fig. 6. Top view of measurement path and positions for the major experiment.

III. Results and Discussion

Figure 7 shows electric field intensity changes when the reference water tank moved along each measurement path shown in Fig. 4, representing the increase and decrease in signal strength from the baseline (where the tank did not exist). Each curve was created from a plot of the average of 40 measurements at each point. The light blue rectangle in the figure is based on the width of the water tank and is considered the ideal response. Signal strength for every curve was greatest while the tank was sandwiched by the two antennas, possibly due to the relative permittivity of water of approximately 70 at the frequency used.

The signal strength peak was maximized when the water tank was moved along Paths 1 and 9. The patterns of the two curves were similar. Peak strength decreased with an increase in distance from the water tank to the closer antenna. When the water tank was located on Path 5, peak signal strength was at its lowest in the middle of the two antennas. The ratio of the maximum and minimum peaks was about 2:1 (0.044:0.023) in the linear scale.

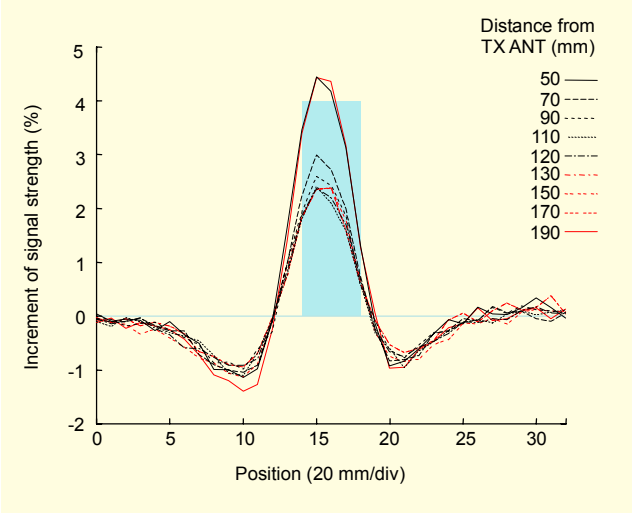

Fig. 7. Changes of signal strength by the reference water tank in the measurement plane.

1. Digital Equalizer

Ideally, regardless of the distance from the antennas, the rectangle response should possess a width equivalent to the light blue rectangle in Fig. 7. However, fluctuations in signal strength, blurring and distortion of back projections, and other artifacts were common. In the figure, the legs as represented by the curves were wider than the actual width of the water tank. In addition, the ends of the legs dropped into the negative region before gradually returning to the baseline. Compensation was necessary to adjust the measurement response to correspond to the tanks' actual shape.

According to the previous report, the response, or measured back projection, of the proposed method was due to the effect of a spatial low pass filter [12]. To compensate for this effect, a digital equalizer was used as a weight function that was designed by an extension of the zero forcing-method (ZF method) because of its simplicity and stability [17].

The method was originally invented to reconstruct distorted waveforms passed through transmission lines. When the response of the delta function through a transmission line was $h_j(-n<j<n)$, its initial distortion D_0 was defined as

$$D_0 = \sum_{j=-n}^{n}{}' |h_j|,$$

where

$$\sum_{j=-n}^{n}{}' |h_j| = \sum_{j=-n}^{-1}|h_j| + \sum_{j=1}^{n}|h_j| \quad \text{and} \quad h_0 = 1.$$

When $D_0<1$, the vector of the tap gains $\mathbf{c}$ was provided by solving

$$\mathbf{Hc}=\mathbf{d}, \tag{1}$$

where

$$\mathbf{H} = \begin{bmatrix} h_0 & h_{-1} & \cdots & h_{-2m} \\ h_1 & h_0 & \cdots & h_{-2m+1} \\ \vdots & \vdots & & \vdots \\ h_{2m} & h_{2m-1} & \cdots & h_0 \end{bmatrix}, \quad \mathbf{c} = \begin{bmatrix} c_{-m} \\ \vdots \\ c_{-1} \\ c_0 \\ c_1 \\ \vdots \\ c_m \end{bmatrix}, \quad \text{and} \quad \mathbf{d} = \begin{bmatrix} 0 \\ \vdots \\ 0 \\ 1 \\ 0 \\ \vdots \\ 0 \end{bmatrix}.$$

Vector $\mathbf{d}$ was the numerical representation of the delta function, and h_j was filled with zero values outside of the measured range.

If tap gain vector $\mathbf{c}$ was obtained in this way, the ZF method provided compensated response $\hat{u}_j$ by the simple calculation

$$\hat{\mathbf{u}} = \mathbf{Uc}, \tag{2}$$

where

$$\hat{\mathbf{u}} = \begin{bmatrix} \hat{u}_{-m} \\ \vdots \\ \hat{u}_0 \\ \vdots \\ \hat{u}_m \end{bmatrix} \quad \text{and} \quad \mathbf{U} = \begin{bmatrix} u_0 & u_{-1} & \cdots & u_{-2m} \\ u_1 & u_0 & \cdots & u_{-2m+1} \\ \vdots & \vdots & & \vdots \\ u_{2m} & u_{2m-1} & \cdots & u_0 \end{bmatrix}.$$

Zero values were filled outside of the measured range of u_j. If

the tap gain vector **c** for the ZF equalizer was properly given first, any response $u_j(-n<j<n)$ was compensated by (2).

The ideal response corresponding to the measured waveforms was the light blue rectangle (not the delta function) shown in Fig. 7. Because **U** and $\hat{\mathbf{u}}$ were known for the reference water tank, **c** was obtained by solving (2). In this case, vector $\hat{\mathbf{u}}$ had elements

$$\hat{u}_k = \begin{cases} 0 & \text{if } k < -2 \text{ or } k > 2 \\ 0.5 & \text{if } k = -2 \text{ or } k = 2 \\ 1 & \text{if } -2 < k < 2 \end{cases}$$

that corresponded to the width of the water tank in Fig. 7. This method was an extension of the ZF method, however; the initial distortion D_0 could not be calculated from the measured values because the input was not the delta function. Therefore, confirmation of result **c** as the optimal solution was not possible. The equalizer was regarded to satisfy the necessary conditions only if its application to measured values resulted in the desired compensation.

In Fig. 7, the peaks and patterns of the two signal strengths almost agreed when the water tank moved along Paths 1 or 9. As the signal strength increment decreased, the signal-to-noise ration became worse because of the increasing distance from the antennas. However, the curves exhibited similar shapes, with differences occurring in amplitude only. Based on these results, an equalizer was designed using the signal strength obtained on Path 1 that provided the best signal-to-noise ratio.

Before calculating the equalizer values, sixteen data points with zero value were added to both ends of the measured data u_j on Path 1 to enlarge the tap order of the digital filter. Finally, tap-gain vector **c**, whose order was 65, was calculated by solving (2).

2. Preprocessing and Applying the Digital Equalizer

Figure 8 shows the relation between the positions of the two water tanks and signal strengths in each direction when the tanks were rotated by π eighth radian (or 22.5°). The value for each point was the average of 20 measurements. Each curve corresponded to a back projection in one direction. The trend was similar to that shown in Fig. 7. However, the difference in maximum to minimum peak signal strength was 6.4 times (5.60:0.87), remarkably larger than that of the reference measurement (2:1). This expansion in signal difference was caused by the closure of the two water tanks to the transmitting and receiving antennas simultaneously, corresponding to Directions 3 and 11 of Fig. 8. For Directions 7 and 15, the two water tanks moved along the path farthest from the antennas simultaneously, making the back projections thin and wide. Peak levels were small, and the tops of the curves were flat. The difference in the signal strengths was expanded by the synergistic effect of these two conditions.

Array **U**, which had 65 by 65 elements, was built from the measured data of each direction by filling zero values outside the measured range. Equation (2) provided compensated response $\hat{\mathbf{u}}$, applying vector **c** that was obtained by the reference measurement.

Figure 9 shows the results of the equalizer application to the measurement for all 16 directions. Because tails were attached to both ends, the horizontal axis had double the space of that

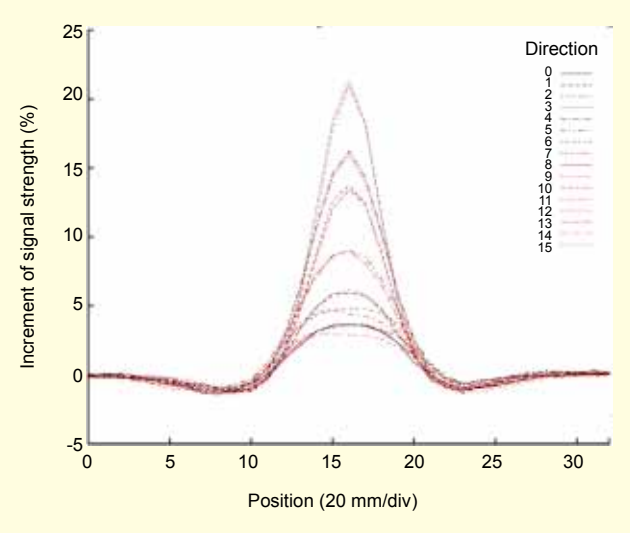

Fig. 8. Relation between signal strength and position of the center of the twin water tanks by 16 different directions.

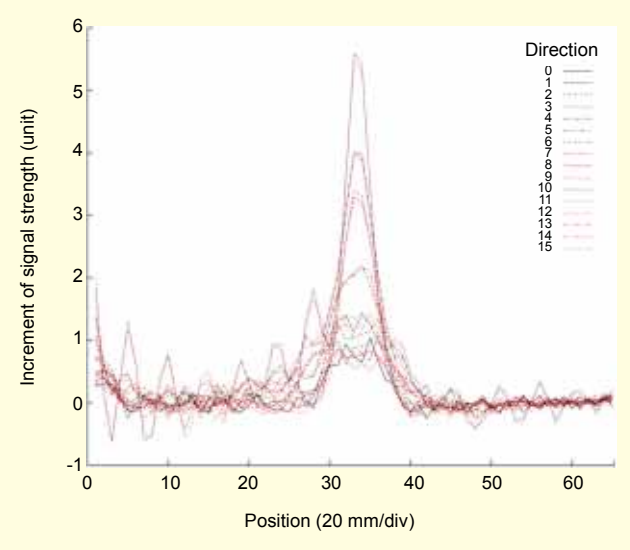

Fig. 9. Relation between signal strength and position of the twin water tank after the equalizer process.

shown in Fig. 8. In general, overshooting into the negative region was eliminated by this compensation. Except for fluctuations in the left domain of Directions 3 and 11 (where the water tank did not exist), no outstanding artifacts were found. Skirts of the curves became narrower and peaks became flatter. The tops of some lower curves separated into two peaks, however; random fluctuations became remarkable when the original signal increment was small. Generally, the effect of the equalizer was apparent, although it could not be confirmed as the optimal solution.

Next, the amplitudes were standardized. If the intensity of the back projection did not have artifacts, the integrations of projection intensity (or increase of electric field intensity) were always the same in every direction. Therefore, a method to standardize the integrations was obtained. Because the equalizer was incomplete, it also caused artifacts. For comparison, other results for which the peak level of each curve was simply standardized were provided.

Two-dimensional images were constructed from the standardized data by simple back projection method. When rotation was applied, the coordinates had errors. To minimize the effect of the coordination errors, the measured curves were oversampled four times after application of the digital equalizer. This process resulted in 257 points for each signal strength curve. The one-dimensional 257-point data was repeated 61 times (or over 30 cm of the span) toward the Y-axis direction to create two-dimensional data. Then, the two-dimensional data were rotated opposite to the measurement rotation by the bi-linear method. Finally, the rotated data of the 16 directions were summed, and the intensity of each point on the measurement plane was obtained.

3. Contours

Figure 10 shows the contour results that were provided by the built-in routine of GNU Octave, a high-level language, primarily intended for numerical computations [18]. For comparison, results without application of the equalizer are also shown. The central areas of 30 cm × 30 cm are shown for all contour plots, and the intensities were standardized within a 0 to 255 gradation. When the equalizer was not applied and data from the 16 directions were simply added, the resulting image contained a gentle peak as shown in Fig. 10(a), and the two water tanks were not distinguishable. However, the direction of the tank alignment and the ridgeline of the contours agreed. When the equalizer was applied, as shown in Fig. 10(b), the peak became long and narrow, emphasizing the ridgeline. In Fig. 10(c), the top of the curve clearly separated into two peaks when the equalized data from 16 directions were standardized by integration. Figure 10(d) also contained two peaks when the equalized data were simply standardized by the peak levels.

The two peaks separated clearly when the data were standardized by integration, and the arrangement of the peaks in relation to the water tanks was acceptable. However, the simple treatment shown in Fig. 10(d) also was effective. No significant differences existed between the two results.

In the experiment using two water tanks that had the same sections but different heights (volumes), the two figures contained two peaks with similar heights. However, the shapes and area of the peaks were different. Further experiments are necessary to determine whether the difference is caused by volume, incompleteness of the equalizer, or another reason.

The simple back projection method reported here was not used in practical computerized tomography because artifacts of unwanted shadows appeared around objects in the re-constructed images. In practical computerized tomography, an appropriate weight function was applied to measured data to eliminate the artifact before the data were summed.

In the proposed method, the weight function was also necessary. At this stage, it was not clear whether the artifact produced by simple back projection was as remarkable as the distortion caused by incomplete use of the equalizer. A weight function to compensate for the back projection artifact was not applied to clarify the effect of the equalizer. Existing reconstruction algorithms should also be explored while improving the equalizer.

Permittivity of water was dominant in the measurements. At room temperature and atmospheric pressure, the relative permittivity of water was approximately 70 at the measurement frequency of 54 MHz; however, changes in temperature and pressure affected the water permittivity. In organs that contain a high amount of water, such as muscles and the bladder, the relative permittivity was approximately 90. In contrast, relative permittivity was estimated at 14 in bone and fat that contained little moisture [4]. The moisture distribution inside the living body produces an image by the method. The fundamental efficiency of the method was confirmed by these experiments. This method can be used for applications appropriate for bio-impedance. However, the resolution of the proposed method needs improvement. Some fundamental aspects of the method, such as antenna design and frequency choice, also need to be optimized.

The necessary transmission power can be decreased if the antenna efficiency improves. Although the transmission power of the current experimental system was low, it was safer to reduce the power and duration of the transmission for human subjects. The duration of the transmission can also be shortened if the measurement mechanism and signal processing are improved.

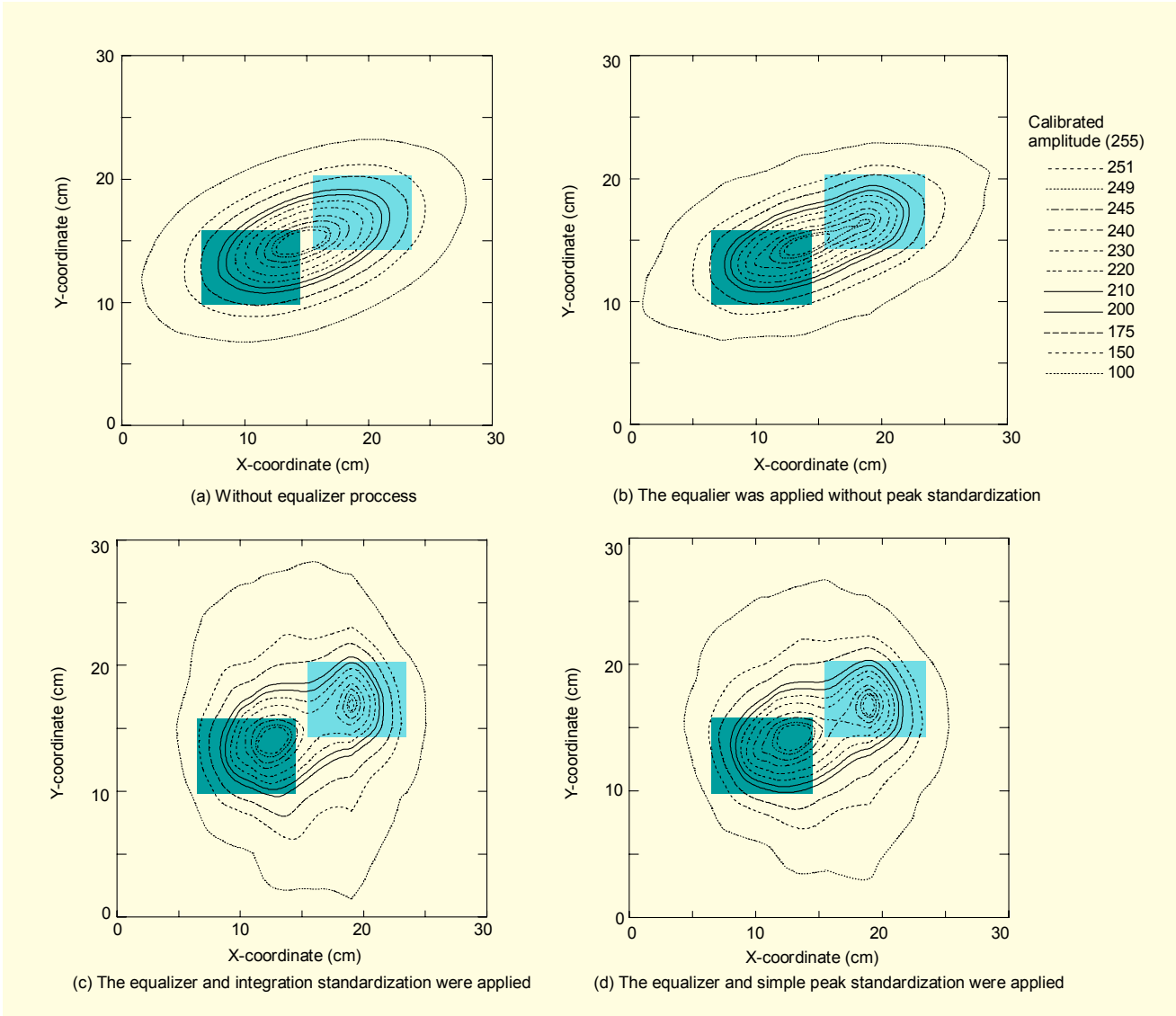

Fig. 10. Reconstructed two-dimensional images of twin water tanks.

Analytical modeling or numerical simulation was helpful to understand the principle of the proposed method and to improve the resolution. This measurement model could not be solved analytically because the dielectric material was located close to the antennas. Therefore, application of the finite difference time domain method [19], a numerical simulation of the electromagnetic field, was under consideration. By this method, the difference would be clarified between the proposed method and magnetic induction tomography [20], [21] that had methodological similarities.

IV. Conclusion

By the measurement and data processing method proposed, discrimination of two water tanks could be obtained in a reconstructed image. This method is applicable to those situations for which bio-impedance is currently being used, such as the monitoring of blood flow, bladder volume, or lung function. Further studies are planned to improve the precision of the reference measurement and to explore the effect of different types of equalizers. Fundamental aspects of the method, such as measurement frequency and antenna design, also require optimizing.

Ideally, the final measurement technique will provide an image of the internal organs of a living human body based on actual moisture distribution in real time.

References

[1] A. Rosen and H.D. Rosen, *New Frontiers in Medical Device*

Technology, John Wiley & Sons, New York, 1995.

[2] L.F. Larsen, L. and J.H. Jacobi, *Medical Applications of Microwave Imaging*, IEEE Press, 1986.

[3] C.C. Johnson and A.W. Guy, "Nonionizing Electromagnetic Wave Effects in Biological Materials and Systems," *Proc. IEEE*, vol. 60, 1972, pp. 692-718.

[4] M. Miyakawa, "Noninvasive Measurement of Temperature Profiles Inside Dielectric Materials," *Bulletin of the Electrotechnical Laboratory*, vol. 45, 1982, pp. 419-435.

[5] G. Rogers, L. Brandt, J. Young, and J. Kot, "The Study of Diffusion Effects in RIM Tomographic Imaging," *Exploration Geophysics*, vol. 24, 1993, pp. 785-788.

[6] L.G. Stolarczyk, R.C. Fry, and T.W. Lloyd, "Radio Imaging Method (RIM) Used to Map Coal Seam Thickness within Developed Longwall Panels," *AAPG Bulletin*, vol. 68, 1984, pp. 951.

[7] L.G. Stolarczyk, "Definition Imaging of an Orebody with the Radio Imaging Method (RIM)," *IEEE Trans Industry Applications*, vol. 28, 1992, pp. 1141-1147.

[8] S. Thomson, J. Young, and N. Sheard "Base Metal Application of the Radio Imaging Method: Current Status and Case Studies," *Exploration Geophysics,* vol. 23, 1992, pp. 367-372.

[9] J. Young, G. Rogers, S. Thomson, and M. Neil, "Australian Development of Tomographic Radio Imaging as a New Tool in Mining Geophysics," *Butsuri-Tansa*, vol. 47, 1994, pp. 249-255.

[10] I. Hieda, "Preliminary Study of Non-Contact Bio-Impedance Measurement by RIM," *Proc. XI Int. Conf. Electric Bio-Impedance*, 2001, pp. 645-648.

[11] I. Hieda, and A. Takahashi, "Relation of Resolution and Distance from Antenna in Medical and Nursing Application of Radio Imaging Method (RIM)," *Proc. Congress of Int. Ergonomics Assoc.*, vol. 5, Aug. 2003, pp. 536-539.

[12] I. Hieda, K.C. Nam, and A. Takahashi, "Basic Characteristics of the Radio Imaging Method for Biomedical Application," *Medical Engineering & Physics*, vol. 26, 2004, pp 431-437.

[13] B.H. Brown, "Impedance Tomography and Spectroscopy: What Can and What Will We See?" *Proc. XI Int. Conf. Electric Bio-Impedance*, 2001, pp. 9-13.

[14] J.G. Webster (Editor), *Electrical Impedance Tomography*, Adam Hilger, Bristol and New York, 1990.

[15] S. Grimnes and O.G. Martinsen, *Bioimpedance and Bioelectricity Basics*, Academic Press, 2000.

[16] J. Sevick, *Transmission Line Transformers*, Noble Publishing, Georgia, 2001.

[17] T. Yahagi, *Theory of Digital Signal Processing 2* (Japanese), Corona Publishing, Tokyo, 1985.

[18] GNU Octave website, http://www.octave.org/

[19] A. Taflove, S.C. Hangness, *Computational Electrodynamics: The Finite-Difference Time-Domain Method,* 2nd ed., Artech House Publishers, Boston and London, 2000.

[20] H. Scharfetty, H.K. Lackner, and J. Rosell, "Magnetic Induction Tomography: Hardware for Multifrequency Measurements in Biological Tissue," *Physiological Measurement*, vol. 22, no. 1, 2001, pp. 131-146.

[21] A. Korjenevsky, V. Cheripenin, and S. Sapetsky, "Magnetic Induction Tomography: Experimental Realization," *Physiological Measurement*, vol. 21, 2002, pp. 89-94.

Ichiro Hieda received the BS, MS, and PhD degrees in electric and electronic engineering from Tokyo Institute of Technology of Japan in 1981, 1983, and 1999. From 1983, he was a researcher of Agency of Industrial Science and Technology (old AIST) in Tsukuba, Japan. From 1996 through 1997, he worked for Australia's Commonwealth Scientific and Industrial Research Organisation (CSIRO) as a Guest Researcher in Sydney, Australia. In 2001, all the institutes under the old AIST were merged into a big research organization, National Institute of Advanced Industrial Science and Technology (new AIST), and as of date, he has been a Senior Researcher of the institute. His main interest is in developing medical equipment for at-home medical care and daily health care.

Ki-Chang Nam received the BS and MS degrees in biomedical engineering from Yonsei University in Korea in 1997 and 1999. He obtained the PhD in biomedical engineering from Yonsei University in Korea in 2004. He was a Research Assistant in the Department of Medical Engineering, College of Medicine, Yonsei University, from 1998 to 2003, and he is currently a Research Fellow.